Chapter 8

Interface Engineering and Electrode Engineering for Organic Solar Cells

Dazheng Chen and Chunfu Zhang

Additional information is available at the end of the chapter

http://dx.doi.org/10.5772/65312

Abstract

Interface engineering and electrode engineering play important roles in the performance improvement for organic solar cells (OSCs). We here would investigate the effect of various cathode modifying layers and ITO-free electrodes on the device performance. First, for inverted organic solar cells (IOSCs) with a poly (3-hexylthiophene-2,5-diyl): [6,6]-phenyl C_{61} butyric acid methyl ester blend, an aqueous solution method using low temperatures is adopted to deposit a ZnO interlayer in IOSCs. When the ZnO annealing temperature is above 80°C, the corresponding IOSCs show senior PCEs over 3.5%. Meanwhile the flexible devices based on poly(ethylene terephthalate) substrate display a PCE of 3.26% and good flexibility. Second, the performance of IOSCs based on AZO cathode and Ca modifier are studied. The resulted IOSCs with an ultrathin Ca modifier (~1 nm) could achieve a senior PCE above 3%, and highly efficient electron transport at AZO/Ca/organic interface, which obviously weakens the light soaking issue. Third, by introducing a 2 nm MoO_3 interlayer for Ag anode deposition, the obtained OSCs show an improved PCE of 2.71%, and the flexible device also achieves a comparable PCE of 2.50%. All these investigations may be instructive for further improvement of device performance and the possible commercialization in the future.

Keywords: organic solar cells, interface engineering, electrode engineering, power conversion efficiency, flexibility

1. Introduction

Organic solar cells (OSCs) have attracted much more attention due to their advantages of low cost, light weight, mechanical flexibility, simple process, and steady improved power conversion efficiency (PCE). Over the past 20 years, many researches about new materials, device structures,

and fabrication processes have been reported for OSCs, and their PCE has remarkably increased from 1% to 10% [1–5]. Nowadays, many efforts have been focused on the further improvement of PCE and long-term stability. Besides the utilizing of novel photoactive materials and device structures, the interface engineering and electrode engineering play important roles in the improvement of device performance and the realization of cost-effective mass manufacture in the future.

In general, the properties of electrode/organic interfaces and transparent electrode materials determine the efficiency of light absorption, charge transport, and collection, which is strongly associated with the open-circuit voltage, short-circuit current density, fill factor, and the overall PCE for IOSCs.

In inverted OSCs (IOSCs), by modifying the indium-tin-oxide (ITO) cathode with functional interface layers and by using high work function metals (Ag, Au) insensitive to air, the IOSCs can obtain improved air-stability while maintaining a PCE comparable to that of conventional structure [6]. Over the past decade, many n-type modifying materials (TiO_2, ZnO) and ultrathin metal films (Ca, Al) have been used to modify the polarity of ITO, so that it can be more effective as an electron-collecting electrode [7–9]. Among these materials, ZnO has a suitable work function, high electron mobility, good optical transmittance, and environmentally friendly nature. Further, it can be prepared by various methods [6, 10], such as the radiofrequency sputtering, atomic layer deposition, sol-gel processing, and so on. All these methods are high cost or high temperature (over 200°C) process, which is not compatible with large area deposition and plastic substrates. For IOSCs, the solution method is time-saving, inexpensive, simple, and compatible with printing techniques and flexible substrates, thus the solution method processed at low temperatures is more desirable. Simultaneously, the ultrathin metal modifier processed by the mature thermal evaporation is also a potential interfacial material, which has been successfully used to modify the ITO cathode and in efficient IOSCs [7, 9].

As we know, ITO is the most commonly used electrode in OSCs; however, the limited reserve of toxic indium element in earth and the increasing price of ITO force us to develop alternatives to ITO. So far, the reported replacements of ITO mainly include the metal films (such as Au, Ag, and oxide/metal/oxide), graphene, carbon nanotubes, and aluminum-doped zinc oxide (AZO) electrodes [3, 11–14]. Among them, AZO is able to meet the requirements of electrode, what is more, Al and Zn are relatively rich in earth, nontoxic and the large area AZO film fabrication is relatively easy. Therefore, the commercial AZO may be more suitable to replace ITO electrode in OSCs. Meanwhile, a smooth and continuous metal thin film (e.g., Ag) can be easily deposited by simple thermal evaporation, suitable for application in the mass production. Moreover, due to their intrinsic flexibility and high conductivity [14], metal thin-film electrodes are also suitable for application in roll-to-roll production of flexible OSCs. It is noted that making the Ag as thin as possible while maintaining its good optical and electrical properties is of vital importance to improve the performance of Ag thin-film electrodes.

In this chapter, besides a simple review of interfacial layers and transparent electrodes, we would like to introduce two efficient modifiers of ZnO and ultrathin Ca films, and two potential ITO-free electrodes of AZO and ultrathin Ag film in IOSCs or OSCs based on poly (3-hexylthiophene-2,5-diyl):[6,6]-phenyl C_{61} butyric acid methyl ester (P3HT:PCBM) blend. Here, not

http://dx.doi.org/10.5772/65312

only the optimization of device parameters, low-temperature process, flexible device, and air stability; but also the energy levels alignment, interface charge transport, metal film growth, light-soaking issue [15], and the underlying mechanism would be investigated. First, an aqueous solution method using low temperature is adopted to deposit a ZnO interlayer in IOSCs. The results show that the transition point of ZnO annealing temperature is approximately 80°C. When the temperature is above 80°C, the corresponding IOSCs show senior photovoltaic performance with PCEs over 3.5%, and the flexible devices based on poly(ethylene terephthalate) (PET) substrates also display a PCE of 3.26% as well as a good flexibility. Second, ITO-free IOSCs based on AZO substrates and ultrathin Ca modifier are studied by optimizing the device parameters and discussing the unexpected light-soaking issue in IOSCs. The results show that IOSCs with an ultrathin Ca modifier (~1 nm) could achieve a senior PCE above 3% and the highly efficient electron transport at AZO/Ca/organic interfaces, which obviously weakens the light soaking issue. Third, by introducing a MoO_3 interlayer for Ag film electrode growth, ITO-free OSCs with a MoO_3 (2 nm)/Ag (9 nm) anode show an improved PCE of 2.71%, and the corresponding flexible device also achieves a comparable PCE of 2.50% to that of ITO-based reference OSCs.

2. ITO-based OSCs with low-temperature ZnO interfacial layer

In this section, IOSCs based on commonly used ITO electrodes and low-temperature solution-processed ZnO interfacial layer are mainly investigated.

2.1. Device fabrication

The aqueous precursor solution used for ZnO production is prepared as follows: ZnO powder (99.9%, particle size <5 μm, Sigma-Aldrich) was dissolved in ammonia (25%, Tianjin Chemical Reagent) to form 0.1 M $Zn(NH_3)_4^{2+}$ solution; then, the solution was ultrasonically processed for 5 min and refrigerated for more than 12 h before use. P3HT and PCBM were purchased from Rieke Metals and Nano-C, respectively. The commercial ITO-coated glass substrate (Zhuhai Kaivo) has a sheet resistance below 10 Ω/square. While the ITO-coated PET substrates show a relatively large resistance (60 Ω/square) and a thickness of 0.15 mm. All the materials are directly used in the device fabrication without any further purification.

Figure 1(a) shows the schematic structure of glass/ITO/ZnO/P3HT:PCBM/MoO_3/Ag for fabricated IOSCs, and the device process was as following: ITO-coated substrates (glass or PET) were ultrasonically cleaned with detergent (Decon 90), deionized water, acetone, and ethyl ethanol, and deionized water for 15–20 min, respectively. Then, the ZnO precursor solution was spin-coated on a nitrogen-dried ITO-coated substrates at 3000 rpm for 40 s and then annealed in an oven at 50, 70, 80, 100, 130, and 150°C for 30 min or 1 h. The deposited ZnO interlayer has a thickness approximately 10 nm. Next, the P3HT:PCBM (1:0.8 wt% in 1,2-dichlorobenzene) solution was spin-coated on ZnO at 1000 rpm for 60 s in a nitrogen-filled glove box. After 150°C preannealing in nitrogen for 10 min, the obtained active layer has a

thickness around 100 nm. Finally, the MoO_3 (8 nm)/Ag (100 nm) anode was thermally evaporated through a shadow mask and the resulted devices have an active area of 10 mm^2.

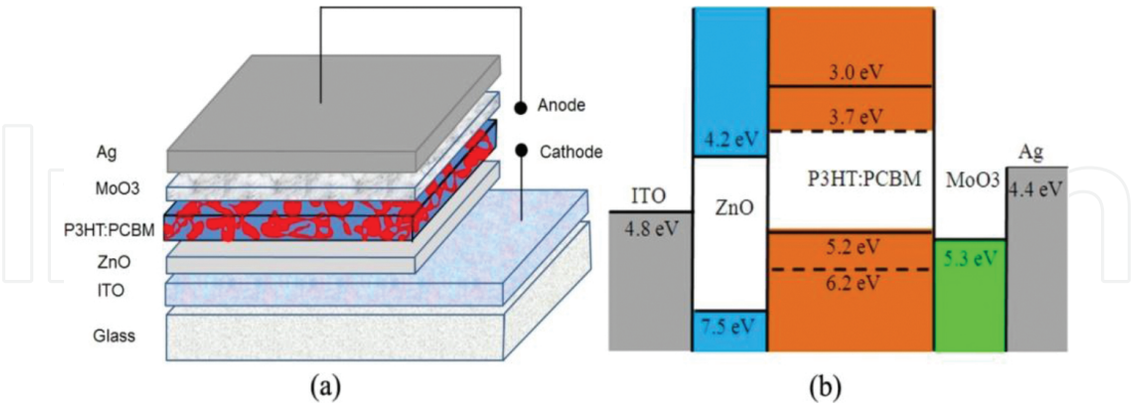

Figure 1. Schematic illustration and ideal energy diagram of materials for the inverted OSCs [6]. Copyright (2015) The Japan Society of Applied Physics.

The current density-voltage (J-V) curves were measured under simulated AM 1.5G solar simulator (Sanei Electric XEC-300M2) using a source-measure unit (Keithley 2400). The illumination intensity is kept at 100 mW/cm^2 using a calibrated Si solar cell. The transmission spectra, film surface morphology, and ZnO film crystal quality were characterized by the ellipsometer (J. A. Woollam WVASE 32), atomic force microscopy (AFM; Agilent 5500), and photoluminescence (PL) spectra (325 nm, He-Cd laser).

2.2. Results and discussion

The fabricated OSCs have a structure shown in **Figure 1**, wherein P3HT:PCBM acts as the photoactive layer, the ZnO film plays the roles of electron transport layer and hole blocking layer. This solution processed ZnO interfacial layer is used to lower ITO work function, modify the ITO polarity, and align the energy levels at ITO/P3HT:PCBM interface. In details, ZnO has the conduction band energy of −4.2 eV and the valence band energy of −7.5 eV, which suggests that electrons from PCBM can be transported into ZnO, while holes from P3HT can be blocked. Meanwhile, the MoO_3 acts as the hole transport layer and electron-blocking layer, and the ITO and Ag play the roles of cathode and anode, respectively.

Figure 2a shows the typical J-V curves under simulated AM 1.5G illumination for IOSCs at different ZnO annealing temperatures. It is well known that the J-V characteristics of solar cells can be described by the single-diode model under illumination, and the relation of J and V is given as follows:

$$J = J_0(\exp(\frac{q(V - R_s J)}{nk_B T}) - 1) + \frac{V - R_s J}{R_{sh}} - J_{ph} \quad (1)$$

where J_0 is the saturation current, q the electron charge, n the ideality factor, k_B the Boltzmann constant, T the temperature, R_s the series resistance, R_{sh} the shunt resistance, and J_{ph} the

http://dx.doi.org/10.5772/65312

photocurrent. Based on Eq. (1) and our previous reported method [16], these photovoltaic parameters extracted from J-V characteristics are shown in **Table 1**. As shown in **Figure 2a**, the experimental data are represented as symbols and the curves calculated from our method are indicated as solid lines. It is clear that the measured data of all devices are well reproduced by the fitting curves.

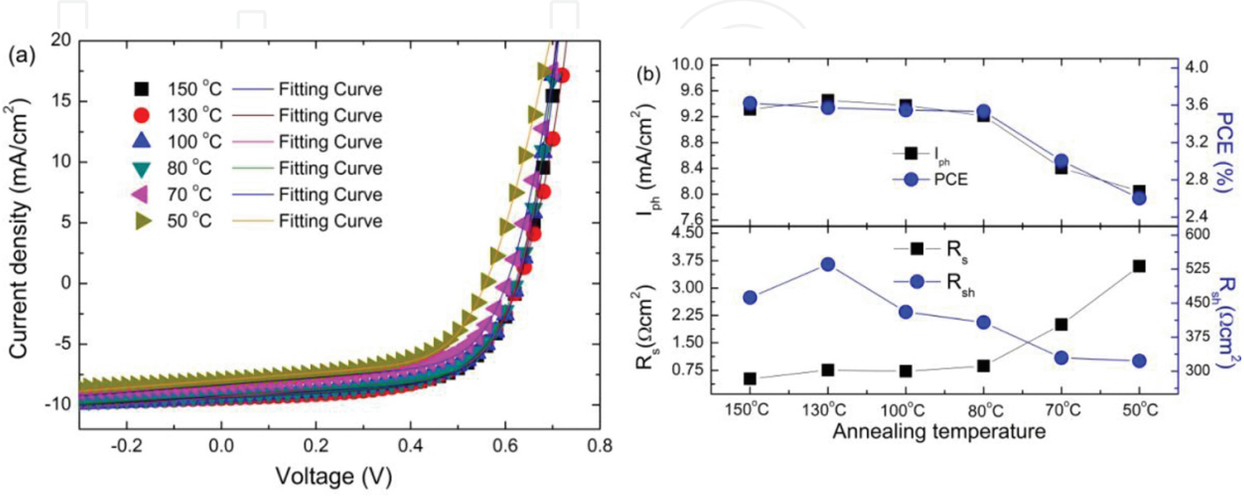

Figure 2. (a) Measured and calculated J-V characteristics of IOSCs with the ZnO interlayer annealed at various temperatures from 50 to 150 °C. (b) Photovoltaic parameters as a function of ZnO annealing temperatures [6]. Copyright (2015) The Japan Society of Applied Physics.

Temperature (°C)	V_{OC} (V)	J_{SC} (mA/cm²)	FF (%)	PCE (%)
150	0.63	−9.30	62.07	3.62
130	0.63	−9.44	60.24	3.57
100	0.62	−9.35	60.66	3.55
80	0.62	−9.19	61.85	3.54
70	0.60	−8.35	59.65	3.00
50	0.56	−7.96	58.57	2.60
Flexible device (80)	0.64	−9.10	56.00	3.26

Table 1. Photovoltaic parameters of inverted OSCs with the ZnO interlayer annealed at different temperatures [6]. Copyright (2015) The Japan Society of Applied Physics.

Figure 2a and **Table 1** show the J-V curves and photovoltaic parameters of IOSCs with ZnO annealed at various temperatures. The device with 150°C annealed ZnO obtains an overall PCE of 3.62% with V_{OC} = 0.63 V, J_{SC} = −9.30 mA/cm², and FF = 62.07%. If the annealing temperature of ZnO decreases from 150 to 80°C, the IOSCs perform well and achieve the almost unchanged PCE of 3.57%, 3.55%, and 3.54 %. However, when the temperature is further decreased (50 or 70°C), the device performance rapidly deteriorates. Although the degradation of the device performance is mainly due to the decrease in photocurrent, it can still be observed

that both V_{OC} and FF also begin to decrease. The effect of the ZnO annealing temperature on the device PCE is also shown in **Figure 2b**. The statistical results in **Figure 3a** show that the temperature approximately 80°C is the transition point, which corresponds to the above discussion. The data are obtained from at least seven devices for each annealing temperature of ZnO interlayer. Meanwhile, the fabricated devices in **Figure 3b** also show good air stability and their PCE could maintain about 90% of the original PCE values after 20 days stored in air.

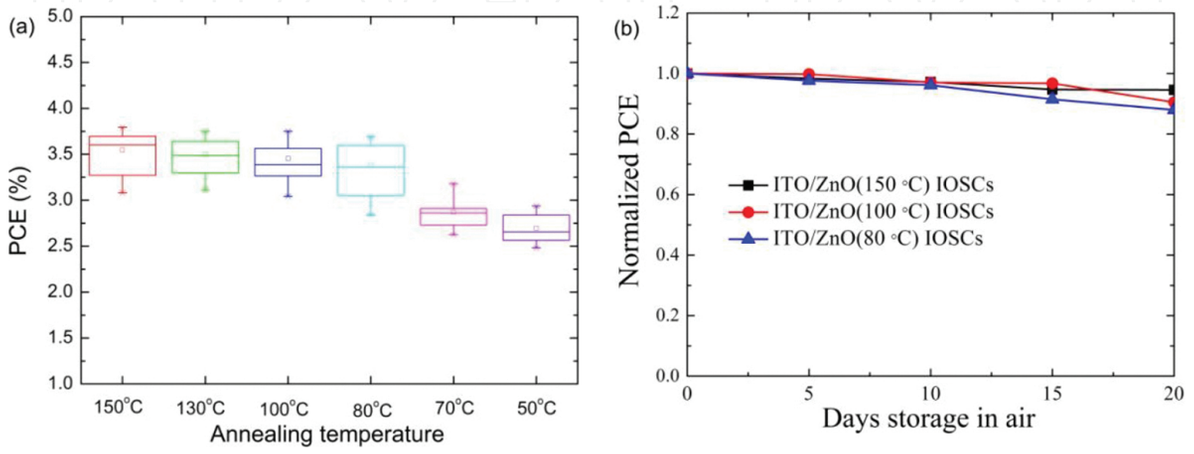

Figure 3. (a) Performance statistical results of the IOSCs with the ZnO interlayer annealed at different temperatures [6]. Copyright (2015) The Japan Society of Applied Physics. (b) PCE degradation of IOSCs in air during 20 days.

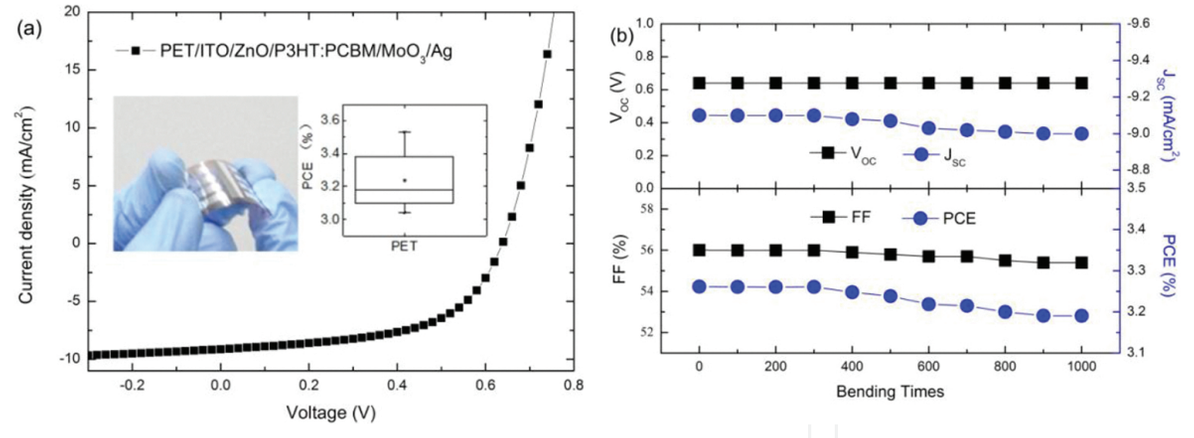

Figure 4. (a) Measured J-V characteristics of and PCE statistical result of flexible IOSCs. (b) Photovoltaic parameters as a function of the number of bending times up to 1000 cycles with a bending radius of about 50 mm [6]. Copyright (2015) The Japan Society of Applied Physics.

Furthermore, IOSCs based on flexible PET substrates were also fabricated with the structure of PET/ITO/ZnO/P3HT:PCBM/MoO_3/Ag. As shown in **Table 1** and **Figure 4a**, the flexible device with ZnO annealed at 80°C shows a PCE of 3.26% with V_{OC} = 0.64 V, J_{SC} = −9.10 mA/cm^2, FF = 56.0%, and the PCE statistical result also shows good device repeatability, which is comparable to that of the reference devices based on glass substrates. Then, the relatively good

http://dx.doi.org/10.5772/65312

ZnO quality achieved at 80°C annealing was again confirmed in the flexible devices. To quantitatively evaluate the device flexibility, a bending test with a number of bending times up to 1000 cycles was carried out. From **Figure 4b**, it could be seen that all the photovoltaic parameters nearly remain unchanged during the first 400 bending cycles, whereas J_{SC} decreases to −9.0 mA/cm^2, FF degrades to 55.4%, and the overall PCE only decreases by 2% from 3.26% to 3.19% after continuous 1000 cycles of bending test. As a result, the device fabricated on flexible PET substrates shows superior flexibility, which proves the potential of low-temperature ZnO deposition method in fabricating flexible IOSCs and other electron devices.

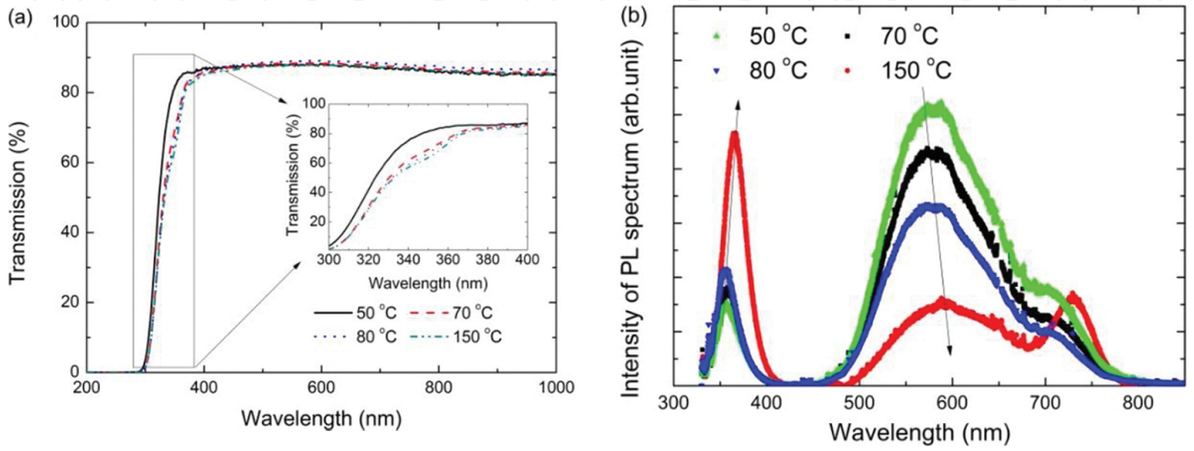

Figure 5. (a) Transmission and (b) PL spectra of ZnO on glass annealed at different temperatures [6]. Copyright (2015) The Japan Society of Applied Physics.

Figure 5a shows the transmission spectra of ZnO/glass samples annealed at 150, 80, 70, and 50°C. All the spectra are very similar and the samples show a transmittance about 88% in the wavelength region from 400 to 1000 nm. And their difference only comes from the shift of transmission edge for ZnO material in the short wavelength region from 300 to 400 nm. It can be seen in the illustration that the transmission edge locates at the lowest wavelength when the ZnO annealing temperature is 50°C and gradually shifts to longer wavelength with the increase in temperatures. Generally, if the material transmittance edge is located at a short wavelength, it has a wide bandgap; otherwise, it has a narrow band gap. A narrow band gap usually means a higher crystalline degree for ZnO [17], so ZnO annealed at higher temperatures has better crystalline quality. From the inset of **Figure 5a**, the relatively smaller shift of the transmission edge for ZnO annealed at 80–150°C means that the ZnO bandgap almost remains unchanged when the annealing temperature is above 80°C, which corresponds to the similar device performance for ZnO annealed at 80–150°C. Meanwhile, from the PL spectra of ZnO in **Figure 5b**, the intrinsic peak in the 350–400 nm range is related to the near-band edge emission of ZnO. With an increase in ZnO annealing temperatures, the intrinsic peak position of ZnO shifts to the longer wavelength and the peak intensity also increases. What is more, the wide peaks in the range from 500 to 800 nm are usually related to the defects in ZnO film, such as interstitial zinc or oxygen atoms, zinc atom vacancy, and oxygen atom or ion vacancy [18]. With an increased temperature, the defect-related peaks are weakened, and thus, the number

of defects is decreased and better ZnO film quality is obtained. Simultaneously, for different ZnO film annealing temperatures of 50, 70, 80, and 150°C, the corresponding root-mean-square surface roughness are 0.673, 0.867, 1.108, and 1.145 nm, respectively. The increased surface roughness corresponds to the more sufficient ZnO crystallization at a high annealing temperature. It is thought that, when the annealing temperature is below 80°C, the ZnO morphology changes markedly, and when the annealing temperature is above 80°C, the ZnO morphology almost remains unchanged. From the morphology results, it is concluded that an annealing temperature of 80°C is sufficient for ZnO crystallization. And the high temperature only slightly improves the film quality, a result agreed to the similar photovoltaic performance of IOSC with ZnO annealed from 80 to 150°C.

According to above discussion, one can draw the conclusion that the 80°C is sufficient for ZnO annealing to obtain a relatively high film quality and act as an interfacial layer, and the resulted devices based glass or PET substrates show the similar photovoltaic performance when the ZnO annealing temperature is higher than 80°C. In short, the senior device performance and good stability show that the aqueous solution method is a more promising low-temperature technique for depositing ZnO in IOSCs and it may be widely applied in flexible and printing devices in the future.

3. ITO-free OSCs based on AZO cathodes and Ca interfacial layer

In this section, ITO-free IOSCs are fabricated on AZO cathodes and ultrathin Ca interfacial layer, the optimization of device performance and light-soaking issue are mainly discussed.

3.1. Device fabrication

The AZO (~980 nm, 2 wt% Al)-coated glass substrates purchased from Zhuhai Kaivo co. were prepared by radiofrequency magnetron sputtering process and they have a sheet resistance of about 7.34 ohm/square and average transmission over 80% in the visible light region. The P3HT:PCBM based bulk heterojunction IOSCs with the AZO transparent cathode was fabricated, and the obtained devices have the structure of Glass/AZO/Ca/P3HT:PCBM/MoO_3/Ag and an active area of 12.5 mm^2. The Ca interfacial modifier with different thicknesses (0, 1, 5, 10 nm) were thermally evaporated on AZO at a base pressure below 5.0×10^{-4} Pa. The detail fabrication process is the same as that in previous section. The J-V characteristics were measured under AM 1.5G solar simulator spectrum before and after 15-min light soaking. The stability of devices was investigated by measuring their J-V characteristics once every 5 days in 1 month.

3.2. Results

From **Figure 6a** and **Table 2**, the AZO only IOSC without an interfacial layer presents a very poor performance and improved V_{OC}, J_{SC}, FF, and PCE after 15 min AM 1.5G continuous illumination (light soaking), shown in **Figures 7a** and **b**. This can be attributed to the energy loss associated with the mismatch of the energy levels between the work function of sputtered AZO (4.5 eV) and the lowest unoccupied molecular orbital (LUMO) level of PCBM (3.7 eV)

http://dx.doi.org/10.5772/65312

(shown in **Figure 8**). During the light soaking, the photogenerated electron-hole pairs in AZO could increase the electron density, fill the trap sites, and thus lower the work function of AZO [15], which improves the electron selectivity from organic layer to AZO cathode and thus induces the improvement of device parameters. However, the performance of AZO only IOSC is still very poor, especially the low V_{OC} of 0.38 V, which indicates that a modifying layer with lower work function must be inserted between AZO and P3HT:PCBM to align their energy levels.

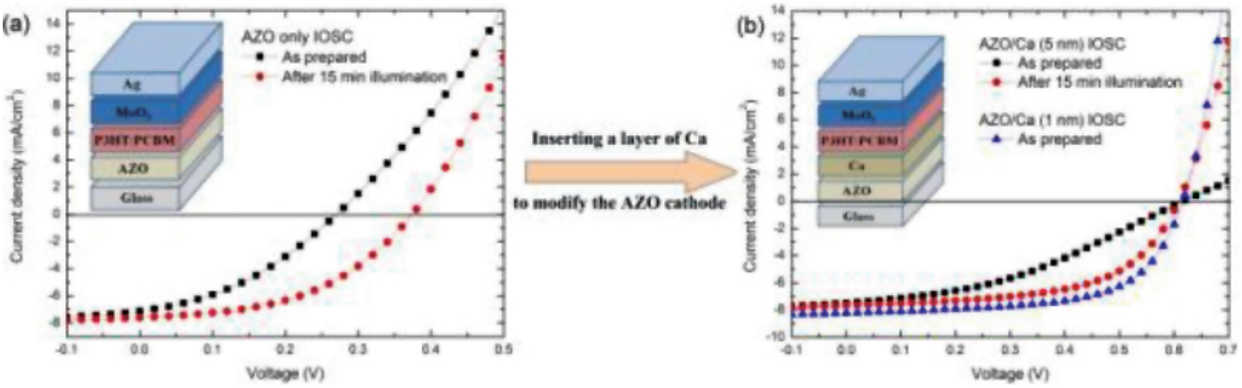

Figure 6. Measured J-V characteristics for as prepared and 15-min illuminated AZO/Ca (0, 1, and 5 nm) IOSCs. Reproduced with permission [20]. Copyright 2014, Elsevier.

Device structures Glass/x/P3HT:PCBM/MoO_3/Ag		V_{OC} (V)	J_{SC} (mA/cm²)	FF (%)	PCE (%)	R_s (Ω cm²)
AZO	As prepared	0.28	−7.11	36	0.72	11.6
	15 min illuminated	0.38	−7.60	46	1.34	4.9
AZO/Ca (5 nm)	As prepared	0.62	−7.49	38	1.74	–
	15 min illuminated	0.60	−7.67	58	2.69	2.3
AZO/Ca (1 nm)		0.62	−8.23	62	3.17	0.7
ITO/Ca (1 nm)		0.64	−7.41	58	2.79	1.5
AZO/Ca (10 nm)		0.62	−7.22	49	2.18	7.1

Table 2. Photovoltaic parameters (PCE, V_{OC}, J_{SC}, and FF) obtained from J-V characteristics of AZO only IOSC, AZO/Ca IOSCs with different Ca thicknesses (1, 5, 10 nm), and the referenced ITO/Ca (1 nm) IOSC. The "–" represents a very large value. For the S-shaped J-V characteristics, the value of R_S is so large that the data are out of the diode model used in the calculation. Reproduced with permission [20]. Copyright 2014, Elsevier.

Then, an electron transport layer of Ca is inserted between AZO and P3HT:PCBM to modify the work function of AZO cathode and the Ca modifier has already been used in ITO based IOSCs [6]. It is clear in **Figure 6** and **Table 2** that, the devices with Ca interfacial layer achieve significant improvement in V_{OC}, J_{SC}, FF, and PCE compared with that of AZO only IOSC. Particularly, an increased V_{OC} (0.60 V) demonstrates that the Ca work function has been pinned to the PCBM Fermi level via the surface states. Consequently, the resulted ohmic contact between Ca and PCBM favors the electron transport and the rectifying contact between Ca and P3HT blocks the hole collection at the AZO cathode. Furthermore, the devices with an ultrathin

Ca (~1 nm) show a superior performance with the highest PCE of 3.17% and lowest R_S of 0.7 Ω cm^2, which is comparable to that of ITO-based device. Thus, the low-cost AZO electrode is one of the promising ITO alternatives.

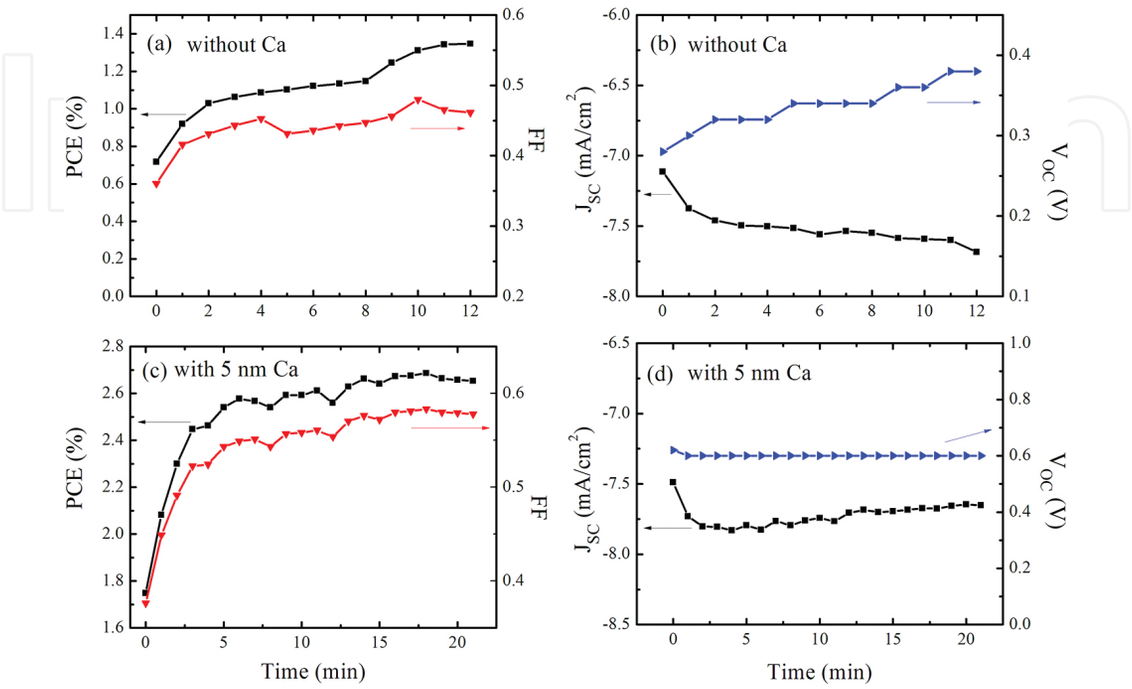

Figure 7. Variations of photovoltaic parameters (PCE, V_{OC}, J_{SC}, and FF) during 15 min light soaking for (a) and (b) the AZO only IOSC, (c) and (d) the AZO/Ca (5 nm) IOSC. Reproduced with permission [20]. Copyright 2014, Elsevier.

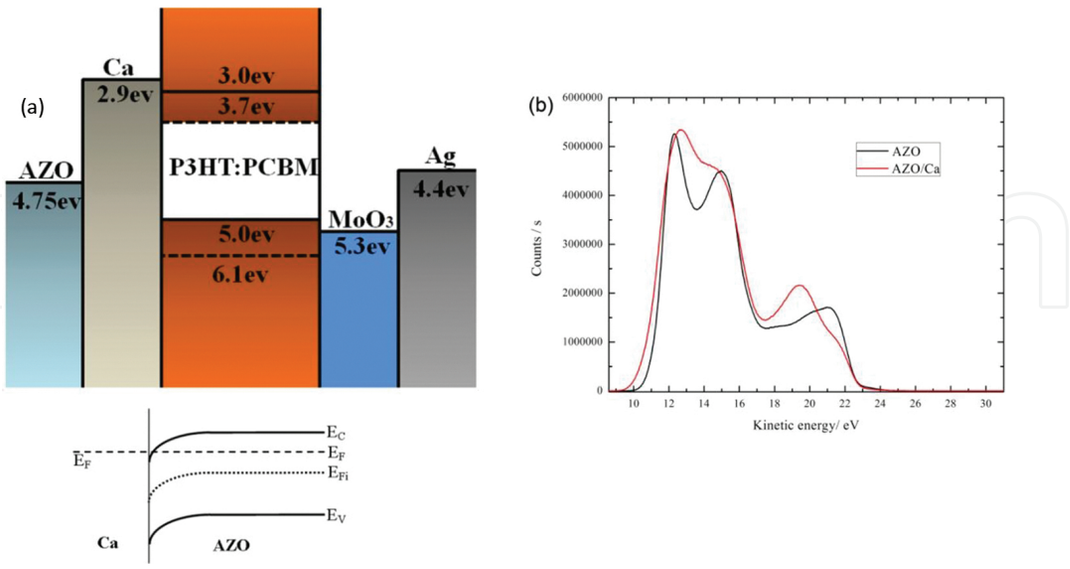

Figure 8. (a) Schematic energy diagram of AZO/Ca IOSCs and ideal band diagram of Ca-AZO contacts according to the ideal metal-n-type semiconductor contact [19]. (b) The AZO work function of 4.5 eV and AZO/Ca work function of 3.8 eV were determined by UPS experiments. Reproduced with permission [20]. Copyright 2014, Elsevier.

http://dx.doi.org/10.5772/65312

One the other hand, for the AZO/Ca (5nm) IOSC, the as prepared device has a low PCE of 1.74% as well as a S-shaped J-V curve, and the PCE increases to 2.69% with the vanish of the S-shaped curve during light soaking, which is observed clearly in **Figures 6b** and **7c**, and **7d**. It is noted that the trend of increasing PCE is nearly identical to that of FF, a slight increase in J_{SC} and nearly unchanged V_{OC} are also observed, which is similar to the reported light-soaking issue [15]. It is obvious in **Table 2** that the R_S of AZO/Ca (5 nm) IOSC shows a remarkable decrease from a very large value to 2.3 Ω cm^2, which is in good agreement with an increase in FF from 38% to 58%. Combining the improved device parameters of AZO only IOSC during light soaking, the strikingly decreased R_S indicates the less energy loss in the charge transport at interfaces and the more efficient charge collection at electrodes. Here, it is thought that the interface electron transport from P3HT:PCBM to AZO is related to the light-soaking issue, which will be discussed in next part. The nearly unchanged V_{OC} demonstrates that an ultrathin Ca layer of 1 nm can also effectively modify the work function of AZO cathode. More remarkably, no light-soaking issue is observed in this device and the detail discussion is shown in next section. Thus, considering the different photovoltaic performances of AZO/Ca (0, 1, 5, and 10 nm) IOSCs, the underlying reasons are deserved to be further investigated.

3.3. Discussion

For a good understanding of different photovoltaic behaviors of AZO-based IOSCs, the following discussions focus on the optical and electrical properties, surface morphology of the AZO/Ca (0, 1, 5, and 10 nm) films. From optical aspect, the transmission spectra of AZO/Ca (x nm) samples in **Figure 9(a)** shows that AZO has a very similar transmission tendency to that of AZO with 1, 5, and 10 nm Ca deposited on it. The lower transmission of AZO/Ca (10 nm) substrate means relatively larger light absorption loss in the active layer, which can be used to explain the relatively poor performance of the AZO/Ca (10 nm) IOSC.

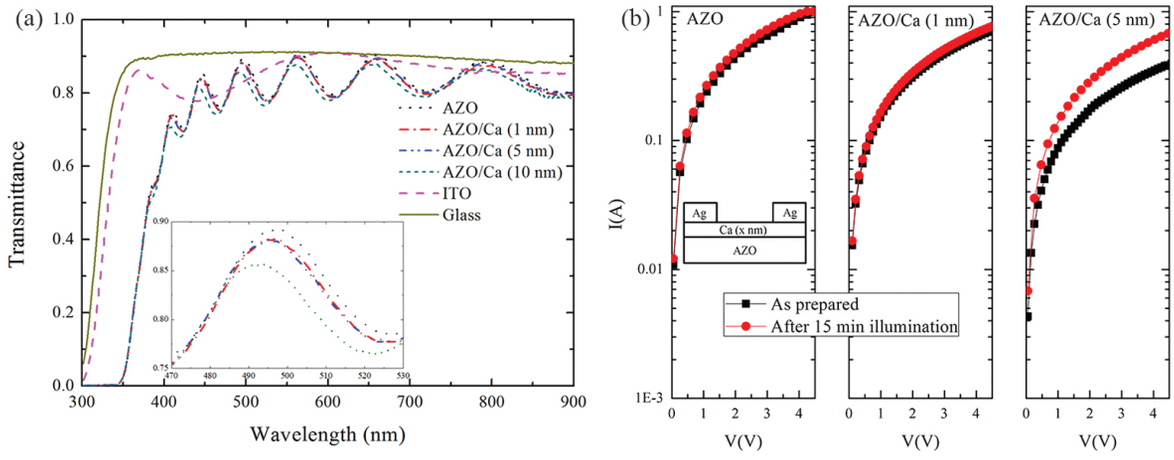

Figure 9. (a) Transmission spectra for the ITO, AZO and AZO/Ca (1, 5, and 10 nm) coated glass substrates. Insert: enlarged pictures for AZO/Ca (0, 1, 5, and 10 nm) substrates in the range from 470 to 530 nm. (b) Photoconductivity measured before and after 15 min AM 1.5 G illumination for the AZO, AZO/Ca (1 nm), and AZO/Ca (5 nm) films on glass substrates. The insert shows the schematic diagram of glass/AZO/Ca (0, 1, and 5 nm)/Ag samples for photoconductivity measurement. Adapted with permission [20]. Copyright 2014, Elsevier.

The coverage of Ca (1, 5, and 10 nm) on AZO films and their surface morphology were characterized by AFM and FE-SEM and no significant differences in morphology could be observed for AZO, AZO/Ca (1 nm), AZO/Ca (5 nm), and AZO/Ca (10 nm) films. This may be related to the very rough surface of AZO films (RMS = 11.59 nm). Fortunately, some useful information may be indirectly acquired from XPS depth profile since the coverage of Ca (1, 5, and 10 nm) on AZO films could be reflected by the different Zn and Ca elements content at the sample surface. The detail XPS analysis and Ca coverage study could be found in our reports [20]. According to the XPS study and the experience Volmer-Weber growth or 3D island growth [21], the AZO film can be completely covered by a Ca layer about 10 nm, while the 1 nm Ca on AZO exists as unclosed islands and the 5 nm Ca could partly cover the AZO surface. From electrical aspect, the measured UPS (He I, 21.2 eV) spectra in **Figure 8** show that the AZO work function (4.5 eV) could be reduced to 3.8 eV by introducing an 5 nm Ca interfacial layer, which is well matched to the LUMO level (3.7 eV) of PCBM. Thus, a Ca modifier can be used to align the energy levels between P3HT:PCBM and AZO cathode.

To further understanding the electron transport in AZO, AZO/Ca (1 nm), and AZO/Ca (5 nm) films, the photoconductivity was investigated as following. It can be observed from **Figure 9b** that the conductivity of AZO and AZO/Ca (1 nm) does not change significantly with the continuous AM 1.5 G illumination; however, the conductivity of AZO/Ca (5 nm) film presents an obvious increase during the 15-min light soaking. From the band diagrams of ideal Ca-AZO contacts shown in **Figure 8**, the different work function between Ca and AZO would cause an electron transport barrier at AZO/Ca interface. For the 5 nm Ca on AZO, the low initial conductivity suggests the large energy loss in the electron transport across AZO/Ca (5 nm) interface, which can be attributed to the electron transport barrier from Ca to AZO as well as the oxidization of Ca layer. During the 15-min light soaking, the photogenerated electron-hole pairs in AZO could increase the electron density, fill the trap sites, and thus lower the work function of AZO, which also lowers the electron transport barrier and improves the electron transport efficiency at AZO/Ca interface, a situation agreed with an increased conductivity of AZO/Ca (5 nm) film and improved J_{SC} in corresponding device. After about 15 min, no further improvement of photovoltaic parameters can be observed and the electron transport reaches a saturated case. For the AZO/Ca (1 nm) sample, its initial conductivity is comparable to the maximum conductivity of AZO/Ca (5 nm) (**Figure 9b**). More importantly, no significant improvement of conductivity is observed upon continuous illumination, which suggests the sufficient charge transport from AZO to Ca. This result is in line with the senior and stable photovoltaic parameters of AZO/Ca (1 nm) IOSC.

According to previous discussion, the high efficient electron transport at AZO/Ca (1 nm)/organic interface may be related to the Ca coverage on AZO. As we know, the 1 nm Ca only exists as isolated islands on AZO surface, and it is thought that the ultrathin Ca may increase the number of active sites, and these isolated sites with low electric potential provide the fast pathway of electron from P3HT:PCBM to AZO. This process may be understood by introducing the Liebig's law of the minimum [22] that the barrel capacity is limited by the shortest stave. Analogously, the active sites may act as the shortest stave and the electrons play the role of water, and the electron prefers to travel through the low-electric-potential pathway provided

http://dx.doi.org/10.5772/65312

by the island-like ultrathin Ca on AZO film, instead of the direct transport across the larger energy barrier at AZO/organic interface. This discussion agrees with the smaller R_S, larger J_{SC}, FF, and PCE of AZO/Ca (1 nm) IOSCs. In other words, the highly efficient electron transport in AZO/Ca (1 nm) film may be responsible for the removed light-soaking issue of as prepared AZO/Ca (1 nm) IOSC. It also should be noted that the unexpected light soaking issue appears after the un-encapsulated device has been stored in air for several days since the oxidation of Ca, but this does not happen for the device stored in N_2. In short, the observed light-soaking phenomenon is strongly related to the electron transport ability at the AZO/Ca/organic interface and the energy loss caused by the oxidation of Ca, and the more exact mechanism should be further investigated in the future work.

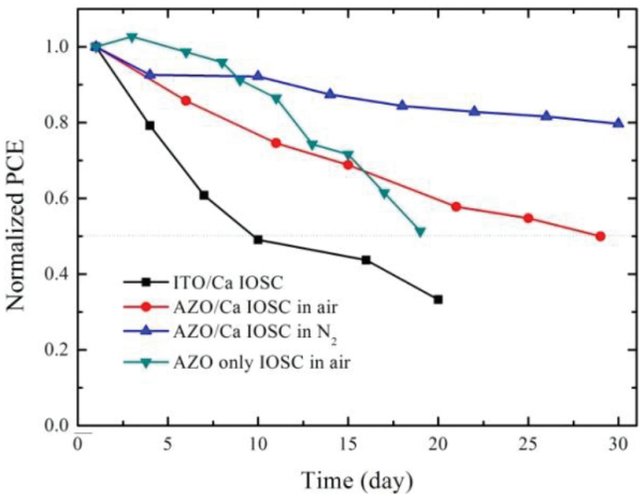

Figure 10. Normalized PCE degradation for AZO/Ca (1 nm) IOSCs and ITO/Ca IOSCs stored in air or N_2. Reproduced with permission [20]. Copyright 2014, Elsevier.

What is more, we investigate the stability of un-encapsulated devices stored in air or N_2 for one month and their normalized PCEs are shown in **Figure 10**. It is very clear that the AZO/Ca (1 nm) IOSC stored in N_2 (measured in air) shows a good stability that its PCE could maintain 80% of the original values after one month. It is noted that the relatively stable V_{OC} demonstrates that the Ca-modified AZO cathode can provide suitable contact for electron collection. Also from **Figure 10**, a degradation of PCE by 50% for the air-stored AZO/Ca (1 nm) IOSC during one month is observed, which can be attributed to the inevitable penetration of oxygen/water from air into the active layer and the oxidization of Ca-modifying layer. Here, the effect of Ca oxidation on the stability could be confirmed from the results of AZO only IOSC. In detail, this device without Ca shows a better stability during the first two weeks in air than that of AZO/Ca (1 nm) IOSC, whereas the mismatch of energy levels at AZO/P3HT:PCBM interface may be responsible for the larger energy loss in charge transport and more un-durable PCE after two weeks. However, the PCE of ITO/Ca (1 nm) IOSC deteriorates by 50% only in 10 days and drops by 80% of the origin values in the next ten days, which further shows the effect of Ca oxidation on the device air-stability. In addition, the increased contact resistance caused by the oxidation and mechanical damages of relatively thin Ag (70 nm) anode

by metal clips during the J-V test may also be a factor of device degradation. As a result, considering the comparable PCEs and better device air-stability, the AZO cathode is a promising alternative of ITO to fabricate the long-lifetime IOSCs.

4. ITO-free OSCs based on Ag thin-film electrodes

In this section, ITO-free OSCs based on (MoO_3/)Ag thin-film electrodes on glass or PET substrates are fabricated, and the best performance of OSCs is obtained by optimizing the thicknesses of Ag film and MoO_3 interlayer. And the underlying mechanism, especially the Ag thin-film growth and film properties are also investigated.

4.1. Device fabrication

The MoO_3/Ag or Ag electrodes were thermally evaporated on glass or PET substrates at a base pressure of 5.0×10^{-4} Pa, with an evaporation rate of 0.02 nm/s for MoO_3 and 0.1 nm/s for Ag, respectively. The thicknesses and evaporation rates of MoO_3, Ag and Al were estimated in situ with a calibrated quartz crystal monitor. Since the 2 nm ultrathin MoO_3 is not smooth and closed, the given thickness had to be a nominal value obtained by the monitor, representing the amount of MoO_3 on the sample. The sheet resistances of these MoO_3/Ag or Ag electrodes were measured by using a four point probe setup system. The transmission spectra were recorded by using a spectrophotometer (Lambda950, PerkinElmer). The fabricated devices has a structure of glass (or PET)/(MoO_3)/Ag/MoO_3/P3HT:PCBM/Al and an active area of 12.5 mm^2. The detail fabrication process is the same as that in previous sections.

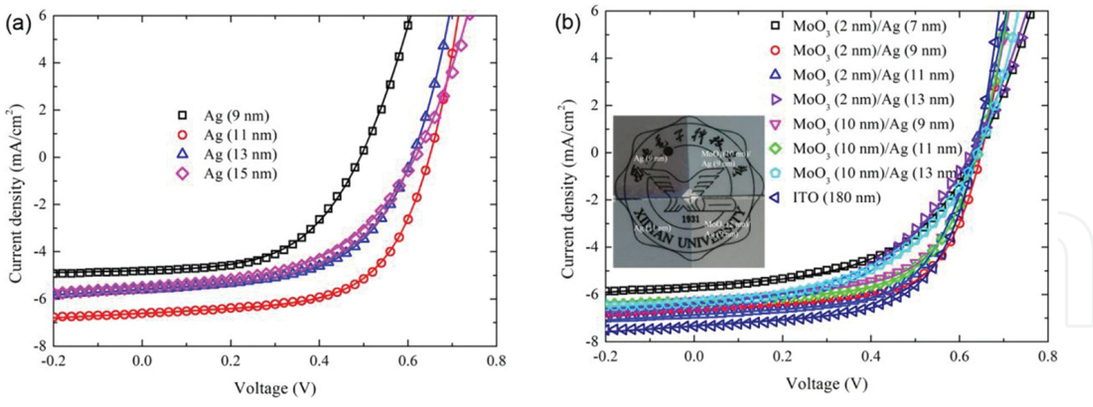

Figure 11. Measured (symbol) and calculated (solid line) J-V characteristics for OSCs fabricated on the (a) Ag or (b) MoO_3/Ag anodes. Inset: A photograph of MoO_3 (2 and 10 nm)/Ag (9 and 11 nm) electrodes. Adapted with permission [11]. Copyright 2014, Elsevier.

4.2. Results and discussion

In details, the OSCs based on Ag thin-film electrode are first fabricated with a structure of glass/Ag/MoO_3/P3HT:PCBM/Al, and then, a MoO_3 interlayer is introduced between glass and

http://dx.doi.org/10.5772/65312

Ag electrode to further improve the device performance. As shown in **Figure 11a** and **Table 3**, the device with 11 nm Ag shows a higher PCE of 2.57% and lower *R*s of 2.0 Ω cm^2. Further, by inserting a MoO_3 interlayer, a senior PCE of 2.71% is obtained by employing a MoO_3 (2 nm)/Ag (9 nm) electrode as well as a relatively low *R*s of 3.0 Ω cm^2, which is comparable to that of reference OSCs based on ITO electrode. Meanwhile, an increase in Ag or MoO_3 layer thickness only degrades the device performance. To understand the underlying mechanism, the optical and electrical properties as well as the surface morphology are studied as follows.

Anodes	J_{SC} (mA/cm^2)	V_{OC} (V)	FF	PCE (%)	*R*s (Ω cm^2)
Ag (9 nm)	4.79	0.49	0.53	1.24	7.5
Ag (11 nm)	6.61	0.65	0.60	2.57	2.0
Ag (13 nm)	5.60	0.61	0.55	1.88	1.9
Ag (15 nm)	5.47	0.62	0.50	1.70	3.6
MoO_3 (2 nm)/Ag (7 nm)	5.67	0.64	0.50	1.82	5.6
MoO_3 (2 nm)/Ag (9 nm)	6.68	0.65	0.63	2.71	3.0
MoO_3 (2 nm)/Ag (11 nm)	6.86	0.63	0.60	2.62	5.8
MoO_3 (2 nm)/Ag (13 nm)	6.41	0.63	0.47	1.90	4.5
MoO_3 (10 nm)/Ag (9 nm)	6.26	0.64	0.59	2.39	3.7
MoO_3 (10 nm)/Ag (11 nm)	6.30	0.64	0.61	2.45	2.8
MoO_3 (10 nm)/Ag (13 nm)	6.26	0.64	0.50	2.02	0.7
ITO (180 nm)	7.33	0.64	0.61	2.85	1.1
PET/MoO_3 (2 nm)/Ag (9 nm)	6.21	0.63	0.64	2.50	–

Table 3. Photovoltaic performance parameters for OSCs fabricated on different anodes/glass substrates. Reproduced with permission [11]. Copyright 2014, Elsevier.

The thermally evaporated Ag film prefers 3D island growth, namely Volmer-Weber growth, which starts from disconnected nuclei [21]. Thus, for the deposition of the first few nanometers of Ag, separate nuclei are formed. According to the SEM images in **Figure 12**, optical transmittance and sheet resistance in **Figure 13**, it can be seen that the percolation threshold thickness of Ag thin film in this study is about 11 nm. At this thickness, the Ag islands are closed and a continuous Ag layer is formed, while the relatively high transmittance and low sheet resistance (6.29 Ω/square) are obtained. This is in good line with the corresponding device performance. By introducing a MoO_3 interlayer, as shown in **Figure 13a**, MoO_3 (2 nm)/Ag (9 nm) anode not only shows similar spectral shape of the transmission curve as Ag (11 nm) electrode but also presents a higher transparency with a maximum of 74% at 361 nm. Particularly, in the visible spectral range, the transparency of the electrode between 56 and 70% is achieved, showing the potential of this electrode. With the introduction of 2 nm thick MoO_3 interlayer between the Ag layer and glass substrate, the sheet resistance of the electrode is decreased to 9.32 Ω/square. The excellent properties of MoO_3 (2 nm)/Ag (9 nm) electrode in

transparency and conductivity lead to the best device performance among all the ITO-free OSCs and verify the fact that the percolation threshold of Ag has been reduced to 9 nm by introducing a 2 nm MoO_3 interlayer. As we know, the thickness of Ag film is strongly related to its transmittance and conductivity, and the percolation threshold thickness determines the smallest thickness for a metal film electrode, which is the most important parameter in the 3D growth of Ag film during the thermal evaporation process. Thus, the decrease in percolation threshold thickness not only could maintain the high conductivity, but also could enhance the optical transmission of Ag film and lower the fabrication cost as well.

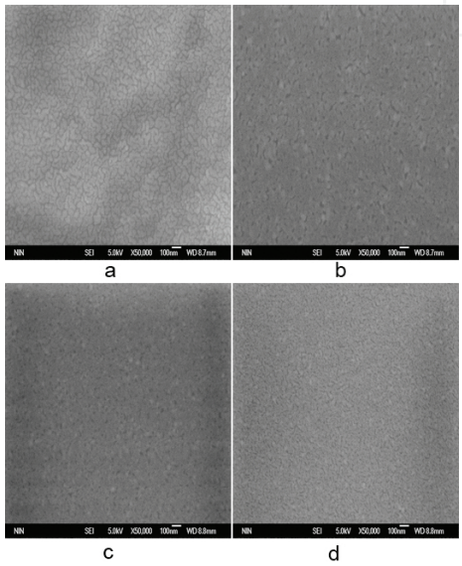

Figure 12. SEM images of (a) Ag (9 nm), (b) Ag (11 nm), (c) MoO_3 (2 nm)/Ag (9 nm) and (d) MoO_3 (10 nm)/Ag (9 nm) electrodes deposited on glass substrates. The white scale bar represents 100 nm. Reproduced with permission [11]. Copyright 2014, Elsevier.

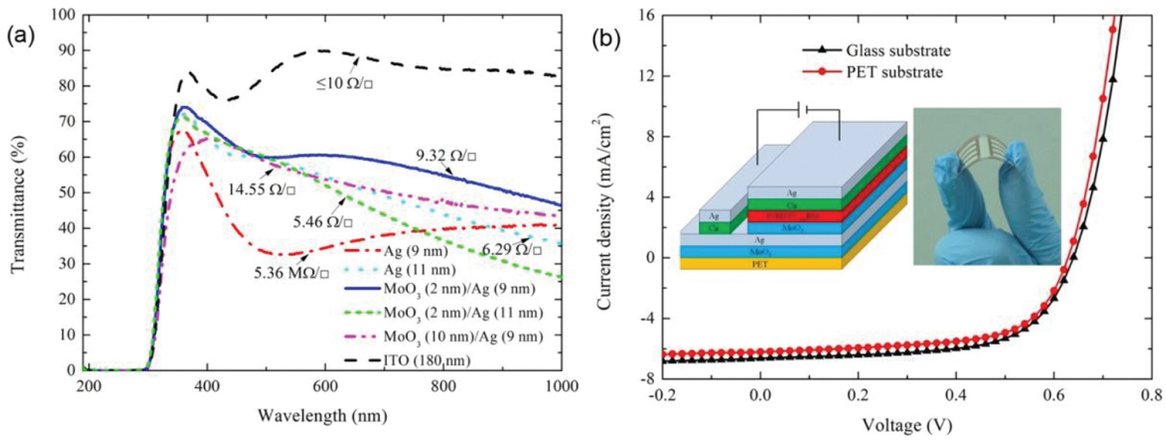

Figure 13. (a) Transmittance spectra with corresponding sheet resistances and (b) J-V characteristics for ITO-free OSCs fabricated on PET or glass substrates. (a) Adapted with permission [11]. Copyright 2014, Elsevier. (b)Reproduced with permission [26]. Copyright 2015, IEEE.

http://dx.doi.org/10.5772/65312

In our opinion, the introduction of the MoO_3 interlayer can effectively improve the wetting of Ag on the substrate and reduce the percolation threshold of Ag. However, the mechanism of the smoothening effect of the MoO_3 layer still remains to be determined. Here, MoO_3 works as a surfactant to modify the surface of Ag film. When the thickness of MoO_3 is 2 nm, the unclosed layer may create preferred nucleation sites on the glass substrate to enhance the lateral growth of Ag film. Similar results are also found in the recent report [23]. However, with an increase in MoO_3 thickness to 10 nm, things become different. Since the surface energy of MoO_3 (γ = 0.06 J m^{-2}) is much less than that of Ag (γ = 1.25 J m^{-2}) [24, 25], the Ag-Ag interactions are stronger than the Ag-substrate interactions, which weakens the surface-modifying effect of the MoO_3 layer. Thus, the effect of a thick MoO_3 interlayer (here 10 nm) on improving the wetting of Ag on the substrate is inferior to that of a thin MoO_3 interlayer (2 nm).

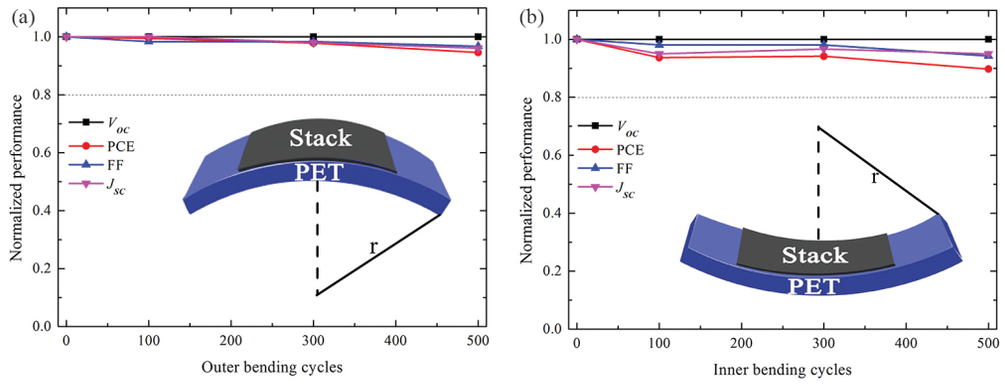

Figure 14. Normalized photovoltaic performance parameters of flexible ITO-free OSCs as a function of the number of (a) outer or (b) inner bending cycles. Adapted with permission [26]. Copyright 2015, IEEE.

Furthermore, flexible devices using our optimized MoO_3 (2 nm)/Ag (9 nm) anode are fabricated on PET substrates with P3HT:PCBM films as the active layer. A PCE of 2.50% is achieved for such flexible ITO-free device (**Table 3**), which is comparable to the PCE (2.71%) of the glass/MoO_3/Ag-based devices and the PCE (2.85%) of glass/ITO-based OSCs. Simultaneously, the corresponding flexible ITO-free OSCs based on MoO_3 (2 nm)/Ag (9 nm) anode show good mechanical flexibility. As shown in **Figure 14**, about 10% degradation in PCE is observed after 500 inner bending cycles with a bending radius of 1.5 cm, whereas a 5% decrease in PCE is observed after 500 outer bending cycles. It shows the huge potential of our flexible electrodes, and it may be instructive for further research on flexible electrodes and roll-to-roll mass production of OSCs.

5. Conclusion

In conclusion, the properties of electrode-organic interfaces and transparent electrode materials have significant impact on the efficiency of light absorption, charge transport and collection, which dominates the overall efficiency of OSCs. Nowadays, the interface engineering and electrode engineering have attracted increased attentions all over the world. In this

chapter, after a simple review of interfacial layers and transparent electrodes reported in OSCs, we have investigated two efficient modifying layers of ZnO and ultrathin Ca films, two potential ITO-free electrodes of AZO and ultrathin Ag film, and their effect on the performance improvement of P3HT:PCBM based OSCs.

By utilizing an aqueous solution method processed ZnO interfacial layer at low temperatures, IOSCs have obtained an obvious improvement of device performance. The results show that the transition point of ZnO annealing temperature is approximately 80°C. When the ZnO annealing temperature is above 80°C, the corresponding IOSCs show senior photovoltaic performances with PCEs higher than 3.5%, and the flexible devices based on PET substrates also display a PCE of 3.26% as well as a good flexibility in bending tests. All devices show good repeatability and air stability. The improved device performance can be attributed to the well-aligned energy levels and improved charge transport between ITO and organic material. Thus, the low-temperature ZnO deposition method based on aqueous solution is a promising technique in fabricating highly efficient IOSCs and flexible devices with long lifetime.

By utilizing an ultrathin Ca modifier and AZO transparent cathodes, ITO-free IOSCs have achieved an obviously improved device performance and weakened light-soaking issue. Although the AZO only IOSC show a very poor performance, IOSCs with a Ca modifier (5 nm or thicker) could obtain the remarkably increased V_{OC} of 0.60 V and PCE of 2.69%, which is attributed to the well-aligned energy levels at AZO/organic interface. When an ultrathin Ca modifier (~1 nm) is introduced, a further improved PCE above 3% is obtained and more importantly, the light soaking issue in the AZO only IOSC and AZO/Ca (5 nm) IOSC has been evidently weakened, which could be explained by the highly efficient electron transport at AZO/Ca/organic interface, while the more exact mechanism should be further investigated in the future work.

By utilizing an ultrathin MoO_3 interlayer for Ag film growth, the MoO_3 (2 nm)/Ag (9 nm) anode not only shows a low sheet resistance of 6.29 Ω/square but also presents a higher transparency with a maximum of 74% at 361 nm, and notably the percolation threshold of Ag film has been decreased from 11 to 9 nm according to the 3D island growth of Ag, confirmed by the SEM, sheet resistance, and transmittance study. The resulted ITO-free OSCs with this MoO_3/Ag anode show an improved PCE 2.71%, and the corresponding flexible device fabricated on PET substrates also achieves a comparable PCE of 2.50% to that of ITO-based OSCs. Thus, the evaporated Ag film electrode with good transmittance and low resistivity is a potential candidate of ITO, and it would find more applications in flexible devices and roll-to-roll production. All investigations in this chapter enrich the understanding of interface and electrode engineering in OSCs, which may be instructive for further research on the improvement of device performance and the possible commercialization in the future.

Acknowledgements

This work is partly financially supported by National Natural Science Foundation of China under Grant 61334002 and 61106063.

Author details

Dazheng Chen* and Chunfu Zhang*

*Address all correspondence to: cfzhang@xidian.edu.cn; dzchen@xidian.edu.cn

State Key Discipline Laboratory of Wide Band Gap Semiconductor Technology, School of Microelectronics, Xidian University, Xi'an, China

References

[1] Yu G, Gao J, Hummelen JC, Wudl F, Heeger AJ. Polymer photovoltaic cells: enhanced efficiencies via a network of internal donor-acceptor heterojunctions. Science. 1995; 270(5243):1789–1791. DOI: 10.1126/science.270.5243.1789

[2] Scharber MC, Sariciftci NS. Efficiency of bulk-heterojunction organic solar cells. Progress in Polymer Science. 2013; 38(12):1929–1940. DOI:10.1016/j.progpolymsci. 2013.05.001

[3] Liu H, Wu Z, Hu J, Song Q, Wu B, Lam Tam H, Yang Q, Hong Choi W, Zhu F. Efficient and ultraviolet durable inverted organic solar cells based on an aluminum-doped zinc oxide transparent cathode. Applied Physics Letters. 2013; 103(4):043309. DOI: http:// dx.doi.org/10.1063/1.4816786

[4] He Z, Xiao B, Liu F, Wu H, Yang Y, Xiao S, Wang C, Russell TP, Cao Y. Single-junction polymer solar cells with high efficiency and photovoltage. Nature Photonics. 2015; 9:174–179. DOI:10.1038/nphoton.2015.6

[5] Chueh CC, Crump M, Jen AKY, Optical enhancement via electrode designs for high-performance polymer solar cells. Advanced Functional Materials. 2016; 26(3):321–340. DOI:10.1002/adfm.201503489

[6] Chen D, Zhang C, Heng T, Wei W, Wang Z, Han G, Feng Q, Hao Y, Zhang J. Efficient inverted polymer solar cells using low-temperature zinc oxide interlayer processed from aqueous solution. Japanese Journal of Applied Physics. 2015; 54(4):042301. DOI: http://dx.doi.org/10.7567/JJAP.54.042301

[7] Shi T, Zhu X, Tu G. Efficient inverted polymer solar cells based on ultrathin aluminum interlayer modified aluminum-doped zinc oxide electrode. Applied Physics Letters. 2014; 104(10):103901. DOI: http://dx.doi.org/10.1063/1.4868101

[8] Lin Z, Jiang C, Zhu CX, Zhang J. Development of inverted organic solar cells with-TiO_2 interface layer by using low-temperature atomic layer deposition. ACS Applied Materials and Interfaces. 2013; 5(3):713–718. DOI: 10.1021/am302252p

[9] Zhao DW, Liu P, Sun XW, Tan ST, Ke L, Kyaw AKK. Indium tin oxide-free and metal-free semitransparent organic solar cells. Applied Physics Letters. 2009; 95(15):153304. DOI: http://dx.doi.org/10.1063/1.3250176

[10] Oh H, Krantz J, Litzov I, Stubhan T, Pinna L, Brabec CJ. Comparison of various sol-gel derived metal oxide layers for inverted organic solar cells. Solar Energy Materials and Solar Cells. 2011; 95(8):2194–2199. DOI:10.1016/j.solmat.2011.03.023

[11] Wang Z, Zhang C, Gao R, Chen D, Tang S, Zhang J, Wang D, Lu X, Hao Y. Improvement of transparent silver thin film anodes for organic solar cells with a decreased percolation threshold of silver. Solar Energy Materials and Solar Cells. 2014; 127:193–200. DOI: 10.1016/j.solmat.2014.04.024

[12] Yambem SD, Haldar A, Liao KS, Dillon EP, Barron AR, Curran SA. Optimization of organic solar cells with thin film Au as anode. Solar Energy Materials and Solar Cells. 2011; 95(8):2424–2430. DOI:10.1016/j.solmat.2011.04.019

[13] Liu ZK, Li J, Yan F. Package-free flexible organic solar cells with graphene top electrodes. Advanced Materials. 2013; 25(31):4296–4301. DOI: 10.1002/adma.201205337

[14] Cao W, Zheng Y, Li Z, Wrzesniewski E, Hammond WT, Xue J. Flexible organic solar cells using an oxide/metal/oxide trilayer as transparent electrode. Organic Electronics. 2012; 13(11):2221–2228. DOI:10.1016/j.orgel.2012.05.047

[15] Trost S, Zilberberg K, Behrendt A, Polywka A, Reckers P, Maibach J, Mayer T, Riedl T. Overcoming the "light-soaking" issue in inverted organic solar cells by the use of Al: ZnO electron extraction layers. Advanced Energy Materials. 2013; 3(11):1437–1444. DOI: 10.1002/aenm.201300402

[16] Zhang C, Zhang J, Hao Y, Lin Z, Zhu C. A simple and efficient solar cell parameter extraction method from a single current-voltage curve. Journal of Applied Physics. 2011; 110(6):064504. DOI: http://dx.doi.org/10.1063/1.3632971

[17] Tan ST, Chen BJ, Sun XW, Fan WJ, Kwok HS, Zhang XH, Chua SJ. Blueshift of optical band gap in ZnO thin films grown by metal-organic chemical-vapor deposition. Journal of Applied Physics. 2005; 98(1):013505. DOI: http://dx.doi.org/10.1063/1.1940137

[18] Wei W, Zhang C, Chen D, Wang Z, Zhu C, Zhang J, Lu X, Hao Y. Efficient "light-soaking"-free inverted organic solar cells with aqueous solution processed low-temperature ZnO electron extraction layers. ACS Applied Materials and Interfaces. 2013; 5(24):13318–13324. DOI: 10.1021/am404291p

[19] Neamen DA. Semiconductor physics and devices: basic principles. 4th ed. Metal-Semiconductor and Semiconductor Heterojunctions. McGraw-Hill. New York. 2011. ISBN-10: 0073529583

[20] Chen D, Zhang C, Wang Z, Zhang J, Tang S, Wei W, Sun L, Hao Y. High efficient ITO free inverted organic solar cells based on ultrathin Ca modified AZO cathode and their

light soaking issue. Organic Electronics. 2014; 15(11):3006–3015. DOI:10.1016/j.orgel.2014.08.042

[21] Sennett R, Scott G. The structure of evaporated metal films and their optical properties. Journal of the Optical Society of America. 1950; 40(4): 203–210. DOI: 10.1364/JOSA.40.000203

[22] Wikipedia. Liebig's law of the minimum [internet]. 2016. Available from< https://en.wikipedia.org/wiki/Liebig%27s_law_of_the_minimum>

[23] Sergeant NP, Hadipour A, Niesen B, Cheyns D, Heremans P, Peumans P, Rand BP. Design of transparent anodes for resonant cavity enhanced light harvesting in organic solar cells. Advanced Materials. 2012; 24(6)728–732. DOI: 10.1002/adma.201104273

[24] Vitos L, Ruban A, Skriver HL, Kollar J. The surface energy of metals. Surface Science. 1998; 411(1–2):186–202. DOI: 10.1016/S0039-6028(98)00363-X

[25] S. Overbury, P. Bertrand, G. Somorjai. Surface composition of binary systems. Prediction of surface phase diagrams of solid solutions. Chemical Review. 1975; 75(5):547–560. DOI: 10.1021/cr60297a001

[26] Wang Z, Zhang C, Chen D, Tang S, Zhang J, Wang Y, Han G., Xu S, Hao Y. Flexible ITO-free organic solar cells based on MoO_3/Ag anodes. IEEE Photonics Journal, 2015; 7(1): 8400109. DOI: 10.1109/JPHOT.2015.2396906

IntechOpen